

A modern Q-meter system to measure the polarization of solid polarized targets ^{*}

P. McGaughey, M. Yurov, A. Klein, D. Kleinjan, K. Liu, J. Mirabal-Martinez

P-25, MS-H846, Los Alamos National Laboratory, Bikini Atoll Road, Los Alamos NM 87545

Abstract

Solid polarized targets are widely used in nuclear and particle physics experiments. Polarization measurements for these targets are normally performed using nuclear magnetic resonance (NMR). The Liverpool Q-meter was developed in the late 1970s and became the de facto standard for these NMR-based measurements. However, it has become increasingly difficult to obtain the required number of Q-meter channels, as the components have become obsolete. The Los Alamos National Laboratory (LANL) high energy nuclear physics (HENP) group has developed a new NMR-based Q-meter system, building upon the basic Liverpool design. The new Q-meter introduces several improvements, such as remote tuning and compact design, while being less costly to produce. These improvements have the potential to increase the accuracy of the polarization measurements, thereby reducing the experimental systematic uncertainties. This modern Q-meter has been successfully tested with both polarized proton and deuteron targets.

Keywords: Q-meter, NMR, polarized target, polarization, nuclear physics, high energy physics

1. Introduction

For many decades high density, highly polarizable solid state targets [1, 2] have been used in nuclear and high energy physics experiments to study spin degrees of freedom. Currently, there are a number of facilities performing experiments using polarized targets, for example: CBELSA/TAPS at ELSA [3], CLAS12 program at JLab [4], COMPASS at CERN [5] and SpinQuest at FNAL [6].

The majority of these targets exploit the process of Dynamic Nuclear Polarization (DNP) to polarize the material. In DNP, a suitable material sample, doped with paramagnetic radicals, is placed in a high magnetic field and is cooled down to low temperature. Under these conditions, the resulting electron polarization of the paramagnetic centers is nearly 100%. The electron polarization is transferred to the nucleus through the hyperfine interaction and the desired spin state is selected by irradiation with microwaves of the appropriate frequency. Since the relaxation time of the nucleon spin is much longer than the one for the electron, the overall polarization of the sample is built up over time.

The most comprehensive description of the DNP process has been achieved with the introduction of the spin temperature concept within the "Provotorov theory" framework [7, 8]. In order to reach a high polarization, highly homogeneous magnetic fields ($dB/B \sim 10^{-4}$) of several Tesla are necessary with a coil geometry optimized to meet the acceptance requirements

of the experiment. The material is maintained at temperatures of about 1 K for operation in *continuous mode* with a ^4He evaporation refrigerator, and below 100 mK in *frozen spin mode* achieved with a $^3\text{He}/^4\text{He}$ dilution refrigerator. The source of the microwave radiation has to be capable of delivering the required power at a frequency near the electron Larmor frequency. For instance, with a 5 T field, a 140 GHz source with a line-width of ~ 10 MHz needs to deliver ~ 20 mW per gram of target material.

The accurate measurement of the target polarization is one of the most critical tasks in these systems. The measuring technique is based on the principle of continuous wave nuclear magnetic resonance (CW-NMR), where a sweeping RF field, applied perpendicular to the axis of the holding field, drives the nucleon spin-flip transitions. The corresponding energy absorbed or emitted is detected by a specially tuned resonant RF circuit, which is connected to the NMR coil embedded in the target material. This circuit, the so-called Liverpool Q-meter, was developed in the late 70s and became the de facto standard for NMR-based polarization measurements of solid polarized targets [9]. However, many discrete components used for the original Q-meter design have become obsolete and re-manufacturing the hardware in its original configuration is no longer possible, as indicated by the authors [10]. Due to the high demand and reduced availability, several groups have worked on developing new NMR systems which would replace the Liverpool Q-meter and potentially add extra functionality [11, 12, 13].

In this paper, a new NMR system to measure the polarization in a solid target is presented, along with an integrated data acquisition system, which was designed by the HENP team at LANL. The development of the new LANL NMR system was driven by the needs of the Fermilab SpinQuest (E1039) experiment [6]. This experiment was proposed by the LANL HENP team to measure the Siverts asymmetry of the nucleon's

^{*}This work was supported by DOE under contract 89233218CNA000001 and LANL LDRD 20130019DR.

Email address: p1m@lanl.gov (P. McGaughey)

\bar{u} and \bar{d} sea quarks in polarized Drell-Yan production for a unique range of virtualities and transverse momenta not accessible in other experiments. The significance of these measurements lies in the fact that a non-zero Sivers asymmetry would be direct evidence for a non-zero orbital angular momentum (OAM) of the light anti-quarks. Current models of the nucleon spin, which do not take into account the contribution from the OAM of the seaquarks, underestimate the nucleon spin by up to 50 % [14]. A sea quark orbital angular momentum contribution to the overall spin of the nucleon would help explaining this discrepancy [15]. By utilizing both proton and deuteron (NH_3 and ND_3) targets, the experiment will also be able to measure a possible flavor dependence of the Sivers function. The ability to obtain high integrated luminosity is paramount to achieving these goals. Therefore, the SpinQuest solid polarized target system design includes up to three 8 cm long target cups on the target ladder. This, in turn, requires the implementation of three NMR channel per cup to properly reflect polarization along the cup axis. Thus, a total of nine new NMR channels (plus spares) is required.

2. Liverpool Q-Meter

The introduction of the Liverpool Q-meter brought significant improvements to the performance and reliability of earlier NMR measurements, which were carried out with a diode demodulator, and had relatively poor linearity as well as an unsatisfactory signal-to-noise ratio. The defining design change was the introduction of RF phase-sensitive detection that provided several important new features: measurement of the real part of the RF signal, noise suppression with respect to the reference frequency and intrinsic linearity of phase-sensitive demodulation.

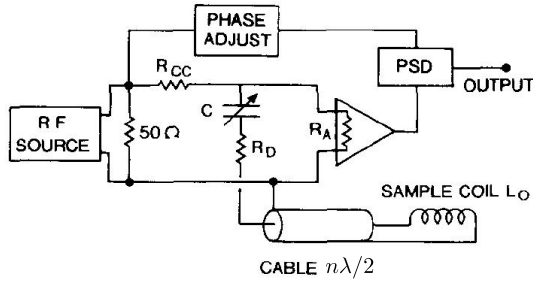


Figure 1: Schematic diagram of the Liverpool Q-meter with a phase-sensitive demodulator (PSD). Figure source: Ref. [9]

The Liverpool Q-meter is a constant-current series-resonant circuit which is sensitive to the changes of the coil quality factor (Q) induced by the polarized nuclei. The schematic diagram of the Liverpool Q-meter is shown in Fig. 1. When describing the Q-meter technique, it is common to use frequency-dependent complex susceptibilities

$$\chi(\omega) = \chi'(\omega) - i\chi''(\omega), \quad (1)$$

instead of the macroscopic magnetization of the target material. The relationship between polarization of the sample and the change in NMR coil impedance, modified by these susceptibilities, is given by:

$$Z(\omega) = R_c + i\omega L_c (1 + 4\pi\eta\chi(\omega)), \quad (2)$$

where ω is the RF field scanning frequency, η is the effective filling factor of the target material within the NMR coil, L_c is the inductance of the bare coil and R_c is the coil resistance. The absorptive (imaginary) part of the dynamic susceptibility is modified by the Zeeman transitions at the nucleon spin-flip resonance and is therefore directly related to the polarization (P) of the target material:

$$P \propto \int_{\Delta\omega} \chi''(\omega) d\omega. \quad (3)$$

At the circuit level, the real part of the (complex) RF voltage across the tuned circuit is measured, which requires phase-sensitive detection. Since the circuit is tuned only at the resonant frequency (ω_0), the off-resonance region of the RF sweep ($\Delta\omega$) has reactive components known as the Q-curve. This background is normally measured by shifting the value of the holding B_0 -field, such that the nucleon resonance position is moved away from the regular sweep range. Furthermore, the combined system of the NMR coil, transmission cable and tuned Q-meter, corresponding to a particular experimental setup, has to be calibrated in order to determine the value of the enhanced polarization. The calibration procedure requires obtaining an NMR signal at conditions where the polarization is known. This condition is typically achieved by thermalizing the nucleon spins with the lattice of the solid target material. The corresponding thermal equilibrium (TE) polarization (P_{TE}) is given by the Boltzmann distribution and can be calculated exactly. The absolute polarization during DNP (enhanced signal) can then be obtained from the integral ratio:

$$P_{enh} = P_{TE} \frac{\int_{\Delta\omega} \Delta V_{enh}(\omega)}{\int_{\Delta\omega} \Delta V_{TE}(\omega)}, \quad (4)$$

where ΔV is the Q-curve subtracted nucleon resonance signal.

A number of conditions dictated by the circuit design and experimental environment have to be satisfied for the optimal operation of the Liverpool Q-meter. A detailed circuit analysis can be found in [9, 16, 17, 18]. The ability to detect small (TE) signals and operate linearly over a very large dynamic range (at least 300:1) is essential for the precise determination of the polarization. One of the most critical parameters in this regard is the absolute value of the NMR coil current. The current has to be low enough to avoid perturbation of the spin state population at TE, yet be sufficient to obtain an optimal signal-to-noise ratio. Running at high values of P , η and B_0 may also lead to conditions where changes in the effective resistance of the NMR coil $\Delta R(\omega)$ become comparable to the input impedance

of the first stage RF amplifier (effectively $50\ \Omega - 100\ \Omega$). In this case, the assumption that the NMR coil RF current is constant is violated and the Q-meter behavior is no longer linear. While the Liverpool Q-meter was originally designed to work at 107 MHz (proton's Larmor frequency at 2.5 T field), its discrete components' frequency response allows operation over a nominal range of 10 MHz – 300 MHz. Therefore, it was successfully used for detecting signals from 16 MHz (at 2.5 T field) for deuterated materials up to 213 MHz (at 5 T field) for hydrogenous materials.

The Liverpool Q-meter module is only one part of the overall target polarization measurement system. The module is housed in a water-cooled, custom-built crate with a separate precision power supply. The Q-meter circuit is driven by an external RF frequency synthesizer with a DAC unit regulating the behavior of a linear RF sweep. The low-frequency (LF) Q-meter output is DC level subtracted and amplified by a standalone unit, commonly known as the Yale card. This amplified signal is digitized by a commercially available ADC. Finally, the synchronization of the DAQ trigger with the RF sweep timing, as well as the DAQ readout, is controlled by a custom developed software package.

3. LANL Q-meter system

The idea behind LANL's new Q-meter design was to offer an easy to operate system that simplifies manufacturing, reduces production cost and provides additional functionality beyond those of the existing Q-meters. The compact architecture of the new system combines all of the necessary infrastructure (NMR analog electronics, fast digitizer and microprocessor with Ethernet interface), which is provided by a minimum set of three printed circuit boards, housed in a standard 6U VME crate, with a capacity of up to six independent NMR channels per crate. An external frequency synthesizer is required to provide the input RF power. State-of-the-art, low-cost signal components with extremely low-noise, low-drift and flat frequency response over a large frequency range are used for the circuit design. A major innovation with respect to the Liverpool system is the use of digital controls for remote tuning. The system features low power consumption ($\sim 5\ \text{W}$ per channel), with little or no cooling required (depending on the ambient environment).

These three custom circuit boards are discussed in the following sections. LANL's analog NMR signal processor board comprises the joint functionality of the Liverpool Q-meter module together with a post-stage LF amplifier similar to the Yale-Card. The Digital Board offers a variety of DAC and ADC services, eliminating the need for a mixture of custom-made digital I/O controllers and industrial DAQ systems. The Controller Board provides VME back-plane communication, as well as data exchange with an external standard desktop computer which runs the LabVIEW control software.

3.1. Analog NMR signal processor

The purpose of the analog board is to provide signal processing and amplification of the RF and LF NMR response in

order to prepare them for digitization. This board is an evolution of the Liverpool Q-meter design, in that it is using a phase-sensitive balanced diode ring mixer to measure the real part of the amplified output of the resonant circuit. Similarly, an additional demodulation channel is provided for magnitude detection and tuning. The board is designed to operate over a frequency range of $\sim 10\ \text{MHz} - 500\ \text{MHz}$, covering the typical signals from both proton and deuterons in high magnetic fields. Careful attention was paid to ensure both a flat frequency and phase response, extremely low noise, large dynamic range and excellent temperature stability. A number of new functional features were introduced, as described below.

- (i) The resonant part of the circuit is built on a separately-shielded external daughter-board, for easy switching to *non-resonant cable* mode of operation.
- (ii) A varactor diode serves as a variable capacitor for remote digital resonance tuning, which is performed by changing the applied voltage (V_{tune}).
- (iii) A phase-shift circuit adjusts the phase of the reference signal by up to 180° or more, which is performed by changing the voltage (V_{phase}).
- (iv) A digital RF attenuator, together with selectable post-mixer LF amplification, allows precise optimization of the overall gain and noise of the system.
- (v) A logarithmic amplifier replaces the diode detector, providing much better linearity and frequency response.

The schematic block diagram of the critical RF and LF sections is shown in Fig. 2. The input RF signal is split into *reference* and *response* paths. The reference signal is supplied to the mixer after the appropriate amplification and phase adjustment, which is provided by a dedicated phase shifter. The frequency tuner employs a varactor diode pair to electronically adjust the tuning capacitance to resonate with the NMR coil inductance. The RF signal gains throughout the circuit are supplied by monolithic microwave integrated circuits (MMICs) and a digital attenuator, which set the signal level to that optimized for the mixer. These MMICs all have a high-gain, low noise ($\sim 0.6\ \text{dB}$) figure and negligible temperature drift. The MMIC amplifiers do have a frequency dependent gain, so a small amount of frequency compensation is applied at the MMIC outputs in the signal chain to flatten the response near higher frequencies (213 MHz). The amplified response signal is routed to the mixer, as well as to the logarithmic detector. The mixer and logarithmic detector outputs are then sent to LF amplifiers. Most of the RF components were obtained from Mini-Circuits and have well specified performance.

The analog printed circuit board has eight metal layers and was designed using the Autodesk electronic design automation software package (EAGLE). The board has a 6U VME format, occupying one VME slot. The VME crate supplies the $+5\ \text{V}$ and $\pm 12\ \text{V}$ rails. An on-board low-noise voltage regulator generates the critical $+3.3\ \text{V}$ used by the MMICs. Most traces carrying RF are $50\ \Omega$ strip-lines, providing excellent shielding.

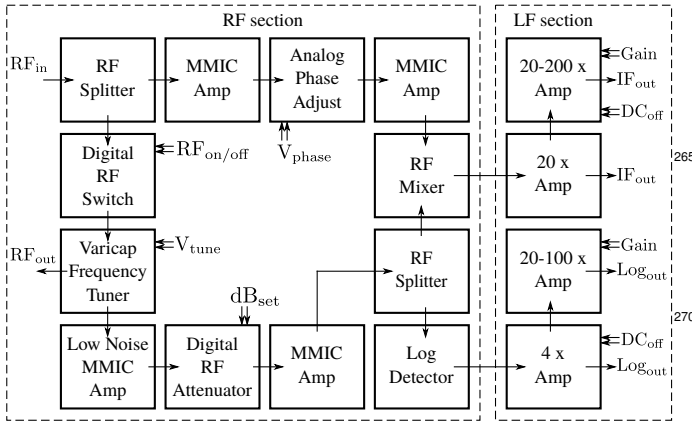


Figure 2: Block diagram of the RF and LF sections of the LANL Analog NMR signal processor. The double arrows indicate user-controllable elements.

Only one inexpensive mechanical shield is required over the section containing the first RF amplifier. In the initial design, the frequency-tuning block resided on the main board. However, subsequent tests showed that the noise performance improves if the frequency tuner is placed in a separate shielded enclosure. Likewise, the operation in the non-resonant cable mode requires the usage of a dedicated external *cold frequency tuner*, as described in the following sections. The circuitry of the phase shifter is contained on a small daughter-card. A photograph of the assembled analog NMR signal processor circuit board is shown in Fig. 3.

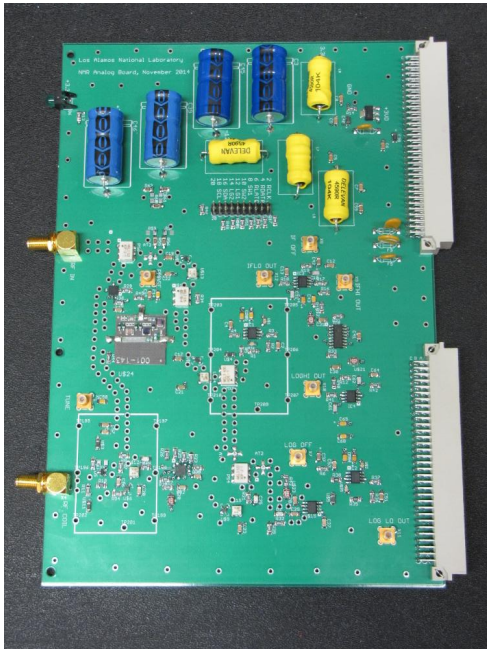


Figure 3: LANL analog NMR signal processor board. Top left coaxial connector (gold) serves as the reference RF input, while the bottom left connector serves as NMR signal input. Connectors (white) on the right side of the board provide the interface to the VME backplane.

3.1.1. External frequency tuner

A separate board was designed to hold the frequency tuner components. A simplified schematic of the board is shown in Fig. 4. The incoming RF from the generator is terminated and converted to a constant current source, with the value of the current (~ 0.3 mA) set by a pair of resistors, R_{IN} and R_{CC} . A varactor diode provides variable capacitance, which is adjusted by an applied 0.5 V– 10 V voltage (V_{tune}), delivering a useful capacitance range of ~ 2 pF– 30 pF. Unfortunately, most varactor diodes exhibit a significant capacitance drift with temperature and have to be temperature compensated. The compensation for the varactor is performed using the negative temperature coefficient of a silicon diode (D_{TC}) in series with the tuning voltage. Fine adjustment of the amount of compensation is achieved by tuning the resistance R_{TC} . After compensation, the center frequency drift with temperature is ≤ 25 ppm/ $^{\circ}$ C, which is usually a small effect. The damping resistor (R_D) sets the minimum resonant impedance to avoid the negative resistance region. Resistor R_{A+} effectively increases the input impedance of the MMIC amplifier to prevent loading down the tuned circuit.

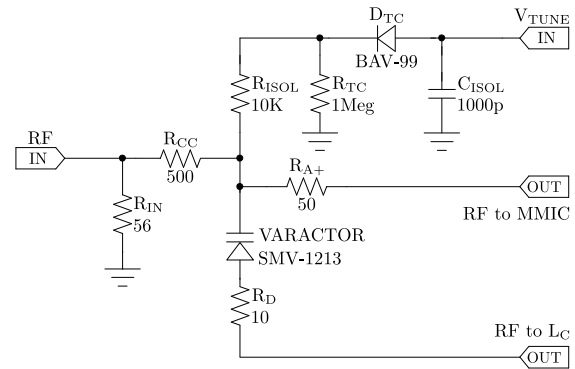


Figure 4: Simplified schematic of varactor-based frequency tuning circuit. The abbreviations used in the circuit diagram indicate: IN=input, CC=constant current, C=coil, ISOL=isolation, TC=temperature compensation, A+=amplifier additional input impedance, OUT=output.

There are two possible mode of operation of the frequency tuner. Traditionally, a $n\lambda/2$ resonant cable connects the remote coil in the cryostat to the tuner circuit. We define this as *warm* operation. The tuner circuitry can instead be placed directly in the cryostat, eliminating the need for a resonant cable [19], which we denote as *cold* operation. The analog NMR signal processor was designed to work in either of these modes without any modification.

Two tuner board variants were designed, one for each mode of operation. The main difference pertains to whether operation is either inside or outside the cryostat. Operation inside the cryostat imposes spatial constraints, and requires operation in a potentially high radiation environment and at extremely low temperature. A photograph of the assembled *warm* tuner circuit board is shown in Fig. 5. The tuner for *cold* operation (not shown) was miniaturized in order to fit the limited space on the target insert ladder. It also carries a regular variable (mechanical) capacitor, as it is expected that semiconductor radiation

damage will prevent the use of a varactor diode (e.g., in E1039). It is, therefore, necessary to perform the LCR tuning procedure prior to placing the target material in the cryostat.

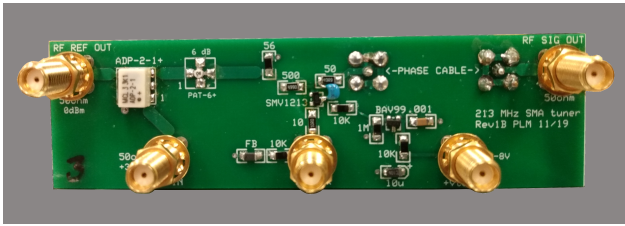


Figure 5: LANL external frequency tuner board. Upper left-hand corner is an RF splitter. Center is a varactor frequency tuner.

3.1.2. Phase shifter

The balanced diode ring mixer is a phase sensitive device that requires a reference RF signal which is in phase with the NMR signal. The phasing of the reference signal is adjusted electronically using an electronic line stretcher and directional coupler [20]. This circuit can electronically shift the phase of an applied signal by over 180 degrees and covers about an octave in frequency, eliminating the need for manually adjusting a phase cable. In order to cover a larger frequency range, more than one phase shifter design has been implemented. The phase shifter for operation near 213 MHz (proton target at 5 T) is composed of a Mini-Circuits line stretcher and directional coupler. This provides an electronically controlled phase shift over a frequency range of ~ 80 MHz – 250 MHz. A dedicated phase shifter was designed to operate at lower frequency for deuteron targets, which covers a frequency range of the ~ 10 MHz – 50 MHz. Both designs were tested and found to not significantly distort the shape of the Q-curve, when operated over an optimum phase adjustment range. Fig. 6 shows the phase shift versus applied voltage for the 5 T proton and deuteron NMR frequencies.

3.1.3. Phase-sensitive demodulator (RF mixer)

Phase-sensitive detection, required for extraction of the real part of the complex RF signal, is achieved by using a double-balanced diode ring frequency mixer. The output of this 3-port device is proportional to the sum and difference of the original frequencies, as well as to the cosine of the phase difference between the two input signals. The mixer output corresponding to the difference of frequencies is selected, which is LF, with the phase difference tuned to be as close to zero as possible. The characteristics of the ADE-1 mixer, used in the LANL Q-meter system, are similar to the one used in the Liverpool Q-meter. Both are level-7 mixers designed to operate in the ~ 0.5 MHz–500 MHz frequency range. The ADE-1 has smaller conversion loss, better isolation between mixer ports and flatter overall frequency response.

3.1.4. Magnitude detection

The LCR circuit has to be tuned to resonance properly before initiating any phase adjustment. Therefore, a conventional

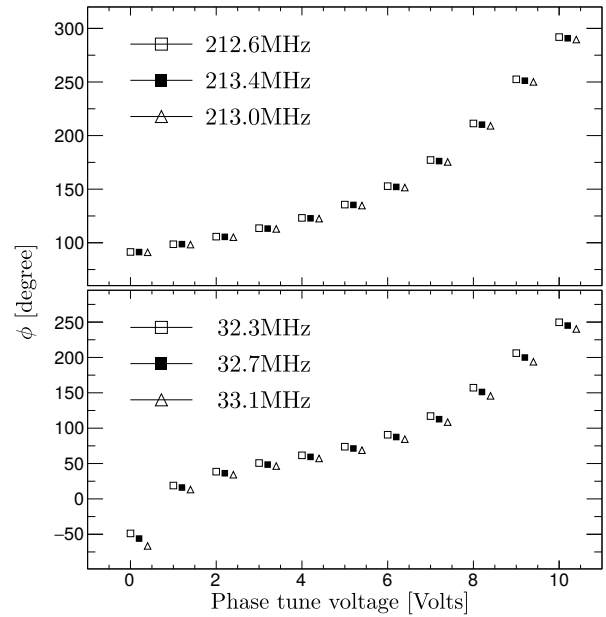


Figure 6: Phase and frequency dependence of the phase shifter versus applied voltage. The phase shift was measured at three frequency settings, as shown in the legend. The data points are shifted by 0.2 V for clarity.

diode detector was introduced in the Liverpool Q-meter design. The LANL Q-meter system, instead, uses a temperature-compensated logarithmic amplifier, providing both improved linearity, dynamic range and frequency response. Its output is the logarithm of the RMS signal power, which includes both the imaginary and real part of the signal, and is mainly used for tuning purposes.

3.1.5. Post-RF amplification

The LF amplification block for both the phase-sensitive and magnitude detection channels was designed to reside on the same analog NMR signal processor board. This is in contrast to the Liverpool system, where a standalone board (Yale-card) was used for post-RF processing. The LF amplification block diagram is shown on the right side of Fig. 2. The outputs of the mixer and logarithmic amplifier are each followed by two stages of operational amplifiers, with programmable gains and DC offsets. Three different levels of LF amplification are available for digitization. The Analog Devices amplifiers used for this purpose have ultra-low noise figure, negligible distortion and excellent DC precision. A small amount of LF shaping is applied to remove any high frequency noise. The four amplifier output signals are carried via coaxial cables to 16-bit ADCs on the digital board.

3.2. Digital processor board

The digital board is a major component of the integrated DAQ system which performs the following three functions: (i) provides the sweep voltage for frequency modulation of the external RF synthesizer; (ii) digitizes the analog LF NMR signals; (iii) controls the analog NMR signal processor board, including the varactor, phase shifter and DC offset; (iv) monitors

system temperature and MMIC voltages. A photograph of the assembled digital circuit board is shown in Fig. 7.

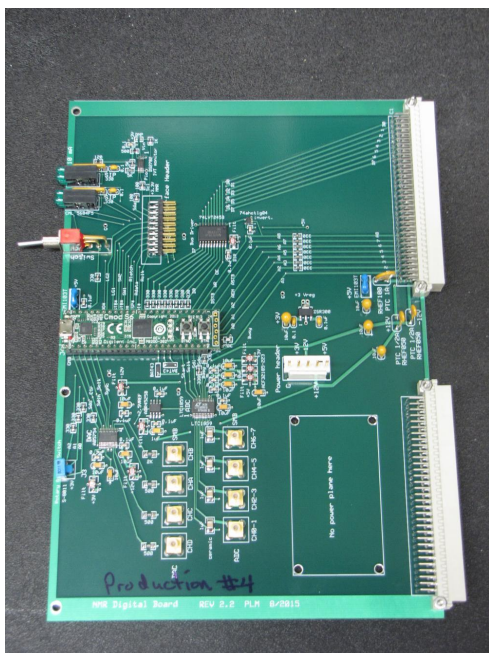


Figure 7: LANL digital processor board. The FPGA daughter-board is located at center-left, with the ADC and DAC converters located directly below.

A block diagram of the digital board is shown in Fig. 8. The hardware components include a four-channel ADC and DAC, controlled by a SPARTAN-6 field programmable gate array (FPGA). The physical layout is a four-layer single-slot VME (6U) printed circuit board.

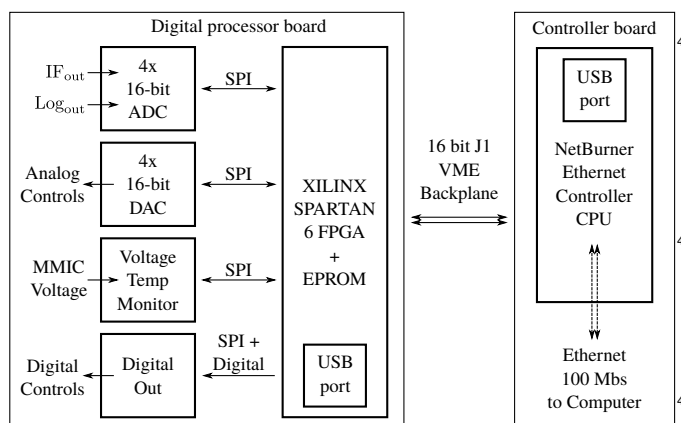


Figure 8: Block diagrams of digital processor and VME controller boards. SPI stands for serial peripheral interface bus.

3.2.1. Digital devices

The on-board four-channel 16-bit bipolar ADC can perform digitization of any one of the demodulation channels at a maximum speed of 100 000 samples/s. It records differential voltage measurements over the ± 5 V range. The ADC has a programmable gain and excellent linearity (< 3 LSB). The high

digitization speed is an important advantage, as most of the noise has a $1/f$ behavior. The four-channel 16-bit bipolar DAC is used to supply the varactor tune, phase shifter, DC offset and RF sweep voltages. A precision voltage reference supplies $+2.5$ V to the ADC and DAC. A separate dual-channel ADC monitors the system temperature and MMIC power supply voltage.

3.2.2. Communication

A Spartan-6 FPGA daughter-board serves as a multiplexer, routing the signals from the attached digital devices through the VME backplane to the crate controller. The FPGA can switch these devices directly onto the VME bus or act as an intelligent processor that accepts commands from the controller and then performs them independently. This flexibility can be used to speed up the data acquisition, as the FPGA can operate at much higher speeds than the controller. The FPGA daughter-board is programmed and tested via a USB connection, with the configuration stored in non-volatile memory (NVRAM).

3.3. Crate controller board

The 6U, dual slot VME controller board is based on a NetBurner system-on-a-module microcontroller. This 32-bit processor runs a real time operating system that is stored in NVRAM. Peripheral interfaces include ethernet, serial ports and a 16-bit bi-directional data bus which is connected to the VME backplane, creating an inexpensive, yet powerful VME system. The microprocessor is programmed in C++ with the included Eclipse editor, GCC compiler and NetBurner software libraries. Telnet communication with a remote computer running LabVIEW is carried over a 100 Mb Ethernet link. The controller can be programmed over Ethernet or USB. After programming or a power cycle, the controller completes booting in just a few seconds. A photograph of the crate controller printed board is shown in Fig. 9.

3.4. Computing

A computer running LabVIEW collects and displays the NMR data. LabVIEW opens a telnet connection to the VME controller, sends a command instruction, waits for the controller to return the data, then processes and displays the resulting signal. Data acquisition speed is currently limited by the controller clock speed at 30 000 samples/s. This can be improved with additional FPGA programming up to the ADC limit of ~ 100 000 samples/s. LabVIEW performs the Q-curve subtraction and background removal from the NMR signal, providing a relatively accurate online polarization measurement. LabVIEW also programs the RF signal generator, using a USB-to-GPIB adapter.

4. Performance tests and comparison with Liverpool Q-meter

4.1. Basic electronic performance

Stray capacitance in the tuner circuitry can result in false tunes, where the constant coil current assumption is violated,

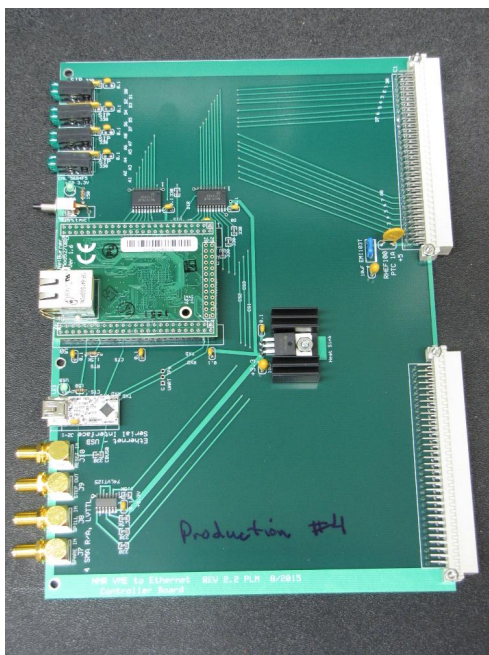


Figure 9: LANL VME crate controller board. The NetBurner micro-processor daughter-board and Ethernet connector are located at center-left. Directly below is the USB interface. Diagnostic LEDs are located at the upper-left hand corner.

435 leading to non-linearities in the NMR response. This is especially important at 213 MHz, where the tuning capacitance is fairly low. The tuner circuitry is built on a section of printed circuit board where all power and ground planes have been removed. The stray capacitance, measured with a network analyzer, was < 1 pF at the varactor output, ensuring series-resonant constant-current operation.

To obtain the best possible signal-to-noise ratio, MMIC amplifiers were chosen that have ultra-low input noise of 0.7 dB vs 2.0 dB for the Liverpool Q-meter amplifier. Using a calibrated noise generator diode, the input excess noise at the varactor diode (without NMR cable and coil) was measured to be < 1 dB. To obtain this noise level, the tuner circuitry required the addition of a metal shield. The noise spectrum with a resonant cable and coil was studied with a spectrum analyzer. Within the bandwidth of the NMR system's output, the low frequency noise spectrum had an $\sim 1/f$ behavior. Optimal NMR performance was obtained by using the fastest possible sweep rate, as was discussed previously.

NMR systems for polarized targets must have a very large dynamic range with excellent linearity. The thermal equilibrium signal for the proton is typically 300 times smaller than that at 100% polarization. The analog NMR signal processor board was designed such that the diode mixer would be the first RF element to approach saturation, as is true for the Liverpool Q-meter. The internal digital RF attenuator allows for precise adjustment of signal levels to remain below this non-linear region.

Accuracy of the polarization measurements is very dependent upon the stability of the NMR system, especially the tune, gain and DC offset. Large shifts in these must be avoided,

otherwise the extracted TE signal area will be strongly affected. The LANL Q-meter system exhibits negligible tune and baseline drift versus time or temperature with a small gain variation of $-0.24\%/^{\circ}\text{C}$. This drift can be accurately removed using either the on-board temperature or offset voltage measurement.

4.2. Tools developed for comparison tests

Careful comparisons between the LANL and Liverpool NMR systems require being able to easily switch a signal source back and forth between them. This switching needs to be done very reliably without disconnecting any cables. A Mini-Circuits high-reliability SPDT RF relay (MSP2T-18XL+) was chosen for this purpose. It has a low and repeatable insertion loss of 0.1 dB for $50\ \Omega$ lines.

Precision dynamic range and linearity studies require accurate amplitude control of RF signals. A digitally controlled RF attenuation system was designed for this purpose. A pair of precision attenuators from Mini-Circuits were placed in series to provide an attenuation range of 0 dB – 63 dB in 0.25 dB steps. The attenuators were programmed by a PC over a 14-bit parallel control bus. These attenuators are fully electronic, providing completely reproducible attenuation with very little phase shift. The resulting amplitude attenuation range of over 1000 covered more than the required dynamic range of the NMR systems.

For tests being done without a polarized target, it was very useful to have a calibrated signal source close to the right frequency and with a line shape similar to the real NMR signal. Fixed and variable amplitude crystal circuits were built for this purpose. The fixed amplitude crystal boxes use an inductively coupled series-resonant surface acoustic wave (SAW) resonator to provide a gaussian-shaped signal at ~ 224 MHz. This SAW device has negligible frequency or amplitude drift, while providing an excellent signal calibration source. The variable amplitude crystal boxes use a capacitively coupled SAW resonator, where a varactor diode provides electronic control of the coupling and hence the signal amplitude, as shown in Fig. 10. A factor of ~ 6 variation in amplitude is available, with the ability to generate strong signals for warm NMR studies. This was particularly useful for warm NMR tests, where the digital attenuator could not be used. The crystal boxes usually generate two well separated peaks, with a strong signal at the series resonant frequency and a weak one at parallel resonance.

4.3. Comparison of Liverpool and LANL NMR systems

The linearities of the LANL and Liverpool cold NMR systems were measured at 224 MHz using the large signal crystal box, 63 dB variable attenuator and RF relay. A crystal was inductively coupled with an NMR coil to produce a pair of large initial signals. The strong signal arises from the series resonance of the crystal, while the weaker signal at higher frequency is the result of a parallel resonance. The resonant part of the circuit was common to both NMR systems, thus allowing comparison of the entire post-LCR electronics, eliminating tuning and $n\lambda/2$ cable effects. Two high-precision 7-bit digitally controlled RF attenuators in series provided a wide dynamic range. A low loss electronically controlled RF switch was used for

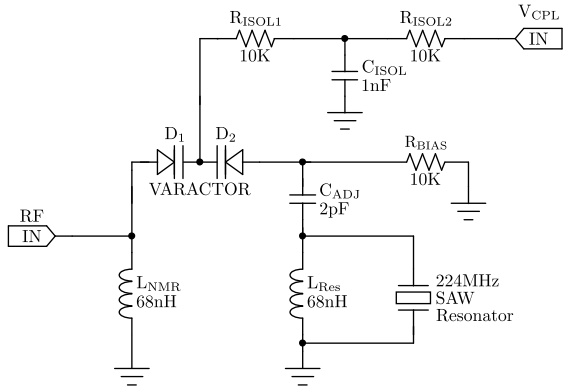


Figure 10: Schematic diagram for variable amplitude crystal signal generator. The abbreviations used in the circuit diagram indicate: IN=input, Res=resonator, ISOL=isolation, ADJ=adjustment, CPL=coupling.

rapid switching between the LANL and Liverpool Q-meters. An amplitude scan on the crystal signal that covered a 60 dB ($\sim \times 1000$) range was performed in 3 dB steps. Example spectra, taken with both strong and weak crystal signals, combined to cover a larger dynamic range, are shown in Fig. 11. After background subtraction and amplitude normalization, the signal shapes from the two Q-meter systems were nearly identical.

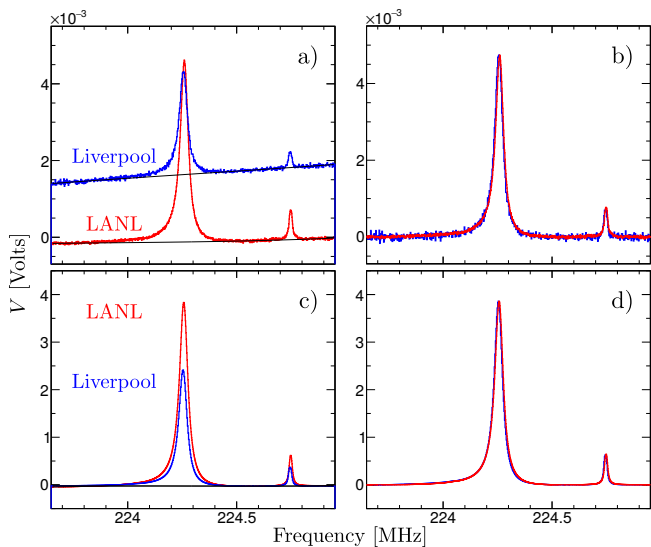


Figure 11: Crystal NMR signals: a) large attenuation (weak, TE-like) raw signal; b) same as a, extracted signal; c) small attenuation (strong, enhanced-like) raw signal; d) same as c, extracted signal. The extracted signals were normalized to the same peak amplitude.

The signal areas of both peaks were individually integrated and plotted versus effective attenuation, as shown in Fig. 12. The data points at the highest attenuation correspond to the weak crystal signals, where the attenuation values have been normalized according to the relative strength of the weak and strong signal peaks. The fitted slopes (p_1 values in Fig. 12) from the two systems are in excellent agreement ($\sim < 1\%$). Both NMR systems exhibit some non-linearity (saturation) for signals above the operating region. Note that the LANL system has an internal attenuator that can be adjusted for optimum

signal-to-noise and linearity. In addition, both systems exhibit a linear dynamic range of at least 70 dB, which is more than adequate for the full range of possible polarizations. The LANL system has improved noise performance, which is visible at the largest attenuation settings.

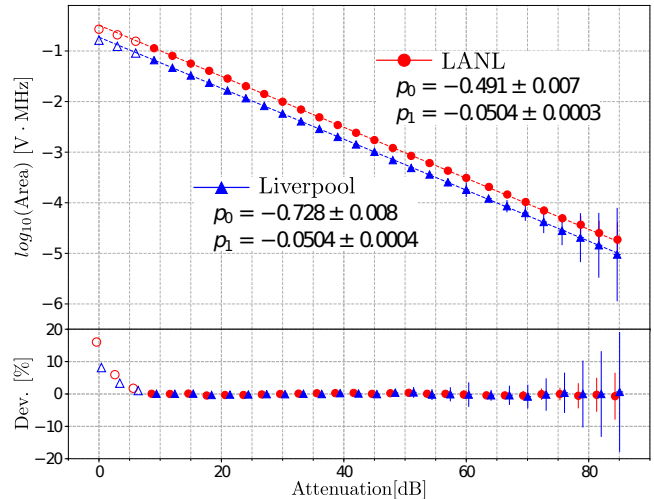


Figure 12: Top: crystal signal area as a function of attenuation for the LANL and Liverpool Q-meter systems. Bottom: deviation from linear fit for the two systems (the corresponding plots are shifted horizontally for clarity). The solid circles indicate the range of the linear fit.

A comparison test of the LANL and Liverpool Q-meters was carried out by observing the proton polarization signal from a NH_3 sample under the normal ($B_0 = 5$ T, $T \sim 1$ K, $\omega_0 = 213$ MHz) conditions. Both systems shared the same NMR coil through the low-loss electronically controlled RF switch. The $n\lambda/2$ cable was also common to both systems, except for the small portion that was split to facilitate connection of the corresponding module. Due to experimental constraints, the NMR cable length was very long ($15\lambda/2$). The thermal equilibrium signal for the proton at ~ 1 K, measured with both systems, is shown in Fig. 13.

The centroid frequency and lineshape are nearly identical for both systems. When normalized at the peak amplitude, the LANL system has lower background noise. The data shown in the figure correspond to an equivalent number of frequency sweeps for both systems. The proton target's polarization was ramped fully positive three times and negative twice, with a maximum positive polarization of $\sim 90\%$ and negative of $\sim 80\%$. The two NMR system's measured polarizations track each other almost perfectly, as also shown in Fig. 14. The overall polarization agreement between the two systems is excellent and within the systematic uncertainties. In order to determine if the polarization showed a dependence upon the applied RF level, the level was reduced by 3 dBm (a factor of 1.4 in voltage). Fig. 14 shows that the resulting normalized polarization values are still in good agreement with the Liverpool Q-meter measurements.

The ability of the LANL Q-meter system to detect extremely small proton signals has been studied by observing the TE-like response from the NH_3 sample as it warms up from ~ 1 K.

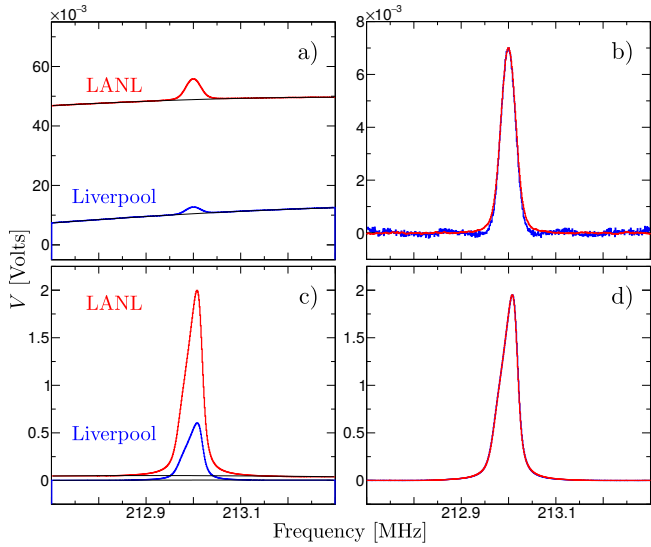


Figure 13: Proton NMR signals at $B_0 = 5$ T: a) TE signal after Q-curve subtraction; b) extracted TE signal; c) signal at high polarization after Q-curve subtraction; d) same as c, extracted signal. The extracted signals were normalized to the same peak amplitude.

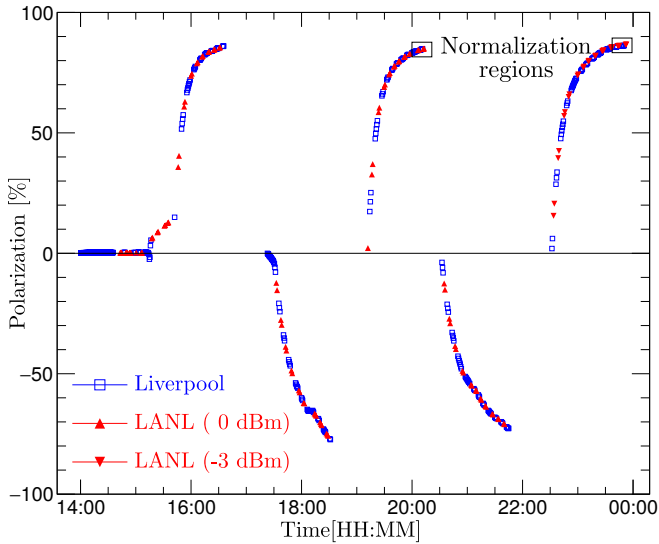


Figure 14: Comparison of polarization measurements for the LANL and Liverpool Q-meter systems during several polarization ramps, both positive and negative. The polarization values were normalized at the indicated regions. Also shown are LANL measurements taken with reduced RF drive level (-3 dBm) during the last positive polarization ramp.

The NMR signal is clearly observed beyond 15.0 K, where the amplitude had decreased by a factor of ~ 20 . Even at this weak signal level, the signal-to-noise ratio is still acceptable.

4.4. Cold mode NMR

A LANL analog NMR signal processor board was setup for cold operation at 32.7 MHz, which is the deuteron NMR frequency at 5 T. A small external constant-current tuning circuit was constructed, containing the NMR coil and a mechanical variable capacitor for tuning. The capacitor was first adjusted for resonance at room temperature, then the circuit assembly

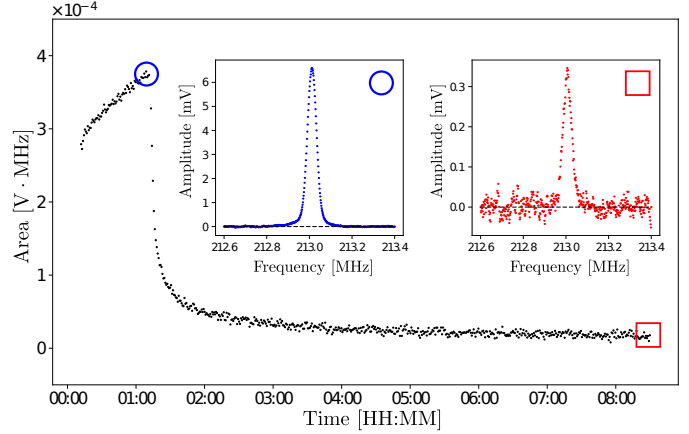


Figure 15: Measurement of extremely small (TE-like) proton signals with the LANL Q-meter system. The NH_3 sample eventually warms up, as the refrigerator is put on standby. The NMR signals shown in blue circle (red square) correspond to ~ 1.2 K (> 15.0 K). The signal plots correspond to an average of 500 double-sweeps.

was placed in liquid nitrogen and returned. After installation in the polarized target, together with a deuterated butanol sample, the deuteron signal was clearly observed at moderate polarization. Fig. 16 shows the measured quadrupole-broadened deuteron signals. Due to the limited cool-down time, the overall (RF and LF) gain of the system was not optimized for the deuteron signal.

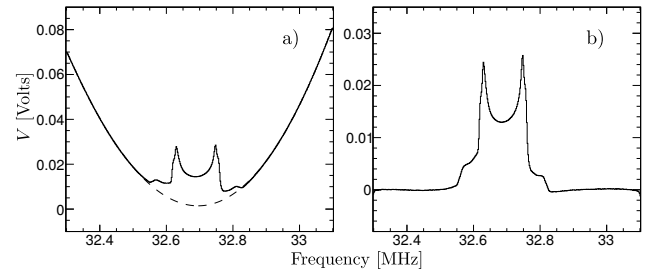


Figure 16: Enhanced deuteron NMR signal from the LANL Q-meter system (cold mode): a) raw signal and fitted background, b) extracted signal.

5. Advanced capabilities

LANL's new design has eliminated all of the manual adjustments used previously by the Liverpool Q-meter (with the exception of tuning the $n\lambda/2$ cable length to the coil). Since the tune, phase and offset are all adjusted electronically, several improvements to the NMR measurements are possible.

5.1. Electronic RF gain adjustments

The analog NMR signal processor board contains a digitally controlled RF attenuator, which allows for precise optimization of the overall RF gain of the system. It adjusts the dynamic range appropriately for a given nuclear species and filling factor of the NMR coil. This new flexibility allows a single board design to serve in a wide variety of experimental conditions.

5.2. Automatic baseline removal

LabVIEW monitors the DC signal baseline from the mixer and automatically adjusts the offset voltage on an even-by-event basis to keep at zero. The offset voltage is directly proportional to the average RF signal level and is therefore a useful monitor of any amplitude or gain shift in the NMR system.

5.3. Synchronous resonance and phase tuning

Extracting a small thermal equilibrium signal superimposed on a large Q-curve background has always been difficult and is one of the primary systematic errors in polarization measurements. The Q-curve can be measured and subtracted by shifting the magnetic field enough to move the polarization signal out of the spectrum. In practice, the various sources of drift due to temperature shifts, field changes and other effects leave a significant background in the signal spectrum, which must be removed.

The magnitude of the Q-curve can be greatly reduced by synchronously adjusting both the tune and phase voltages, for resonance and phase match, at each frequency step during the sweep [21, 22]. First, one determines the correct tune voltage at each frequency using the logarithmic detector output, thereby creating a table of correction voltages. After applying this correction, the mixer output signal would be studied to obtain correction voltages for the phase voltage. Once both corrections are applied, the Q-curve is largely removed from the raw NMR signal. These corrections can be handled by either the VME controller or the FPGA. A major advantage of this method is the possibility of increasing the overall system gain and improving the signal-to-noise ratio.

5.4. Measurement of both the real and dispersive parts of the NMR signal

The electronic phase shifter is capable of moving the phase of the mixer reference signal by 180° . Normally, the phase is adjusted to obtain the real part of the signal, for which the signal area is proportional to the polarization. When the phase is further shifted by 90° , the resulting signal is a measure of the dispersion. This can be accomplished by simply changing the phase voltage for those sweeps. Dispersion can affect the NMR signal shape, complicate the area extraction and cause non-linearities. The nonlinear effects arising under certain conditions, outlined in [16, 17], can be treated with this imaginary part of the signal detection. While several solutions, such as the use of full waveform digitization or an additional phase-sensitive detection channel, were suggested to address this problem, their implementation has not yet been accomplished.

5.5. Cold and warm NMR capability

While *warm* NMR is a good approach for the proton thermal equilibrium signal, it is more challenging to observe the much weaker TE signal of the deuteron. This can be remedied by instead using a *cold* NMR system where all of the resonance tuning components are placed next to the coil inside the cryostat. Two signal cables are now used, one to bring in the strong

RF sweep signal to the coil and another to bring back the weak NMR signal.

Therefore, deleterious effects due to cable attenuation, temperature-dependent dielectric properties, large asymmetric reactive impedances in the off-resonance region and induced noise, that would degrade NMR signal quality, can be largely eliminated. Another benefit of the *cold* NMR is the reduction of the Johnson noise in the cooled LCR part of the Q-meter. As was mentioned earlier, the LANL Q-Meter has been shown to operate in both configurations. Operating in *cold* mode with a very low noise amplifier and a high sample rate will enable improved NMR measurements for the deuteron.

6. Future Work

At present, the LANL Q-meter system uses a NetBurner MOD5270 microprocessor to control the data acquisition electronics. This processor resides on the controller card in the VME crate and communicates over the backplane with the digitizer cards. Currently, most of this communication is done serially, directly to the ADC and DAC converters. Limitations in the speed of the microprocessor I/O bus result in an effective communication speed of ~ 1 Mb/s. However, each digitizer card has an on-board FPGA that could perform the parallel to serial data conversions and independently control the data converters. This method has the potential to increase the data throughput by about an order of magnitude, by having the backplane data transfers be parallel rather than serial.

As a test case, one of the digitizer FPGAs was programmed to internally compute and generate the frequency ramp signal, requiring only step commands from the microprocessor. This software change alone doubled the overall data throughput of the NMR system. Further FPGA code development should provide at least another factor of two speed improvement. In addition, development of the appropriate FPGA firmware would enable new functional features, such as synchronous resonance tuning, synchronous phase tuning and dispersive detection, as outlined earlier. Having the FPGA directly control the digitizers can also enable fast synchronous multi-coil operation, again by reducing the load on the controller.

Further improvements are possible by upgrading the microprocessor to newer models with higher clock speeds. For example, NetBurner now provides an ARM cortex microprocessor with twice the clock speed of the one currently used. Another low cost option is the Raspberry Pi 4 single board computer which has a very fast quad-core 1.5 GHz CPU. New controller board layout and software would be required for either of these upgrades.

7. Conclusions

A new system has been developed to measure the polarization of solid polarized targets using NMR. This work was initially motivated as a cost effective, high density replacement of the aging Liverpool Q-meter for the E1039/Spinquest experiment at FNAL. The LANL Q-meter system includes both a

modern RF phase-sensitive Q-meter and a fully integrated DAQ unit. Major modifications have been included in the LANL system to allow for electronic tuning and gain adjustments. Introduction of a varactor diode to replace the mechanical tuning capacitor and addition of an electronic phase shifter allow full remote control of both resonance and phase tuning.

Use of a multi-layer printed circuit board with modern, state-of-the-art components, results in a compact and cost effective implementation, where standard VME crates are used to house and power the system. A 6U VME crate can carry up to six NMR channels, which can be operated in a time-sequential switching mode, with the RF power provided from a single RF source. Introduction of a digitally controlled RF attenuator adds the flexibility of precise gain adjustments, in order to provide optimum performance for a particular experiment. These hardware improvements provide an opportunity to address the design limitations outlined by the authors of the traditional Liverpool Q-meter system [10, 21, 23]. In particular, the new LANL NMR system has the potential to realize both synchronous resonance and phase tuning, in order to minimize the background for small signal detection. In addition, it becomes possible to detect the imaginary part of the NMR signal by sequential switching of the phase tune setting on every RF sweep. Only firmware and software development is required to implement these newly developed capabilities. Another requirement, that has become almost mandatory for a modern polarization measurement system, is the ability to run in a non-resonant cable mode of operation. This mode, also known as *cold* NMR, is essential for removal of background drift effects and other signal instabilities arising due to variation of the RF cable parameters. This option was incorporated in the LANL Q-meter design at an early development stage and requires no component modifications. A proof-of-principle *cold* NMR test was successfully conducted by detecting the enhanced polarization signal from a deuterated butanol sample.

Key elements of the LANL Q-meter system's performance were first evaluated at LANL, during warm tests with a adjustable crystal signal. The testing continued in several runs during cool-downs conducted by LANL and the polarized target group at the University of Virginia. The system was also tested by the polarized target group at the University of New Hampshire. The emphasis of these tests was on a precise comparison between the LANL and Liverpool Q-meters. The major goal of the comparison was to determine whether both systems return the same results when exposed to the identical input signal. Other goals were to verify the range of linear response and to characterize the relative signal-to-noise ratios.

The LANL and Liverpool Q-meter systems were shown to behave identically ($\sim 1.5\%$), within systematic uncertainties, for both the polarization and crystal tests, after normalization to account for gain differences. Dynamic range studies with a variable crystal signal demonstrate that the range of linear response for both systems exceed 70 dB. The LANL Q-meter system showed similar or better signal-to-noise performance for very small signals, while showing excellent (proton) NMR signal shape agreement with the Liverpool system.

Acknowledgments

This work was supported by the U.S. Department of Energy under contract 89233218CNA000001 and by the Los Alamos Laboratory Directed Research and Development (LDRD) office (20130019DR). We thank Dr. G.R. Court of Liverpool University for helpful suggestions concerning the design of the LANL Q-meter system. We would like to thank the solid polarized target group at the University of Virginia for continuous support, useful discussions and for providing the required infrastructure for tests and measurements. We also would like to thank the solid polarized target group at the University of New Hampshire for testing out the system.

References

- [1] D. G. Crabb, W. Meyer, **SOLID POLARIZED TARGETS FOR NUCLEAR AND PARTICLE PHYSICS EXPERIMENTS**, Annual Review of Nuclear and Particle Science 47 (1) (1997) 67–109. doi:10.1146/annurev.nucl.47.1.67. URL <https://doi.org/10.1146/annurev.nucl.47.1.67>
- [2] S. Goertz, W. Meyer, G. Reicherz, **Polarized H, D and ^3He targets for particle physics experiments**, Progress in Particle and Nuclear Physics 49 (2) (2002) 403–489. doi:10.1016/S0146-6410(02)00159-X. URL <http://www.sciencedirect.com/science/article/pii/S014664100200159X>
- [3] S. Runkel, S. Goertz, H. Dutz, M. Bornstein, **The Polarized Target at the CBELSA/TAPS Experiment**, PoS SPIN2018 (2019) 108. doi:10.22323/1.346.0108.
- [4] C. Keith, **A Dynamically Polarized Solid Target for CLAS12**, PoS PSTP2017 (2018) 008. URL <https://pos.sissa.it/324/008/pdf>
- [5] N. Doshita, et al., **Polarized target at COMPASS**, PoS PSTP2019 (2020). URL <https://pos.sissa.it/379/049/pdf>
- [6] A. Klein, et al., **Letter of Intent for a Drell-Yan Experiment with a Polarized Proton Target** (8 2014). doi:10.2172/1296770. URL <https://doi.org/10.2172/1296770>
- [7] M. Borghini, **Spin-Temperature Model of Nuclear Dynamic Polarization Using Free Radicals**, Phys. Rev. Lett. 20 (1968) 419–421. doi:10.1103/PhysRevLett.20.419. URL <https://link.aps.org/doi/10.1103/PhysRevLett.20.419>
- [8] A. Abragam, M. Goldman, **Principles of dynamic nuclear polarisation**, Reports on Progress in Physics 41 (3) (1978) 395–467. doi:10.1088/0034-4885/41/3/002. URL <https://doi.org/10.1088/0034-4885/41/3/002>
- [9] G. Court, D. Gifford, P. Harrison, W. Heyes, M. Houlden, **A high precision Q-meter for the measurement of proton polarization in polarised targets**, Nuclear Instruments and Methods in Physics Research Section A: Accelerators, Spectrometers, Detectors and Associated Equipment 324 (3) (1993) 433–440. doi:10.1016/0168-9002(93)91047-Q. URL <http://www.sciencedirect.com/science/article/pii/016890029391047Q>
- [10] G. Court, **The development of NMR techniques for the high precision measurement of target polarisation**, Nuclear Instruments and Methods in Physics Research Section A: Accelerators, Spectrometers, Detectors and Associated Equipment 526 (1) (2004) 65–69, proceedings of the ninth International Workshop on Polarized Solid Targets and Techniques. doi:10.1016/j.nima.2004.03.152. URL <http://www.sciencedirect.com/science/article/pii/S0168900204005595>
- [11] J. Herick, **Development of a new Q-meter module**, PoS PSTP2015 (2016) 011. doi:10.22323/1.243.0011. URL <https://doi.org/10.22323/1.243.0011>
- [12] J. D. Maxwell, **Developing New Q-meters for NMR Measurements of Polarized Solids**, PoS PSTP2019 (2020). URL <https://pos.sissa.it/379/051/pdf>

- [13] M. Yurov, P. L. McGaughey, J. Mirabal-Martinez, *A New Target Polarization Measurement System for the Fermilab Polarized Drell-Yan Spin-Quest Experiment*, PoS PSTP2019 (2020).
URL <https://pos.sissa.it/379/059/pdf>
- [14] K. Liu, et al., *Quark and Glue Momenta and Angular Momenta in the Proton — a Lattice Calculation*, PoS LATTICE2011 (2011) 164. doi: 10.22323/1.139.0164.
URL <https://pos.sissa.it/139/164>
- [15] G. T. Garvey, *Orbital angular momentum in the nucleon*, Phys. Rev. C 81 (2010) 055212. doi:10.1103/PhysRevC.81.055212.
URL <https://link.aps.org/doi/10.1103/PhysRevC.81.055212>
- [16] Y. Kisselev, C. Dulya, T. Niinikoski, *Measurement of complex RF susceptibility using a series Q-meter*, Nuclear Instruments and Methods in Physics Research Section A: Accelerators, Spectrometers, Detectors and Associated Equipment 354 (2) (1995) 249–261. doi:10.1016/0168-9002(94)01066-8.
URL <http://www.sciencedirect.com/science/article/pii/S0168900294010668>
- [17] T. Niinikoski, *Topics in NMR polarization measurement*, Nuclear Instruments and Methods in Physics Research Section A: Accelerators, Spectrometers, Detectors and Associated Equipment 356 (1) (1995) 62–73, Proceedings of the Seventh International Workshop on Polarized Target Materials and Techniques. doi:10.1016/0168-9002(94)01446-9.
URL <http://www.sciencedirect.com/science/article/pii/S0168900294014469>
- [18] D. Adams, et al., *The polarized double cell target of the SMC*, Nuclear Instruments and Methods in Physics Research Section A: Accelerators, Spectrometers, Detectors and Associated Equipment 437 (1) (1999) 23–67. doi:10.1016/S0168-9002(99)00582-3.
URL <http://www.sciencedirect.com/science/article/pii/S0168900299005823>
- [19] G. Court, M. Houlden, S. Bltman, D. Crabb, D. Day, Y. Prok, S. Penttila, C. Keith, *High precision measurement of the polarization in solid state polarized targets using NMR*, Nuclear Instruments and Methods in Physics Research Section A: Accelerators, Spectrometers, Detectors and Associated Equipment 527 (3) (2004) 253–263. doi:10.1016/j.nima.2004.02.041.
URL <http://www.sciencedirect.com/science/article/pii/S0168900204006151>
- [20] H. Vondracek, *Entwicklung einer HF-Messschaltung zur Polarisationsdetektion*, Ph.D. thesis, Fakultät für Physik und Astronomie der Ruhr-Universität Bochum, unpublished thesis (2013).
- [21] G. R. Court, M. A. Houlden, *Possible methods to reduce the size of the background signal in continuous wave Q-meters*, Proceedings, The Workshop on NMR in Polarized Targets, Charlottesville, Virginia, April 15-16, 1998. 7–14.
- [22] P. Haulte, *Detection of small NMR signals*, Proceedings, The Workshop on NMR in Polarized Targets, Charlottesville, Virginia, April 15-16, 1998. 54–66.
- [23] G. R. Court, M. A. Houlden, *Modelling non-constant current effects for a series tune NMR Q-meter used for Nucleon polarisation measurements*, Proceedings, The Workshop on NMR in Polarized Targets, Charlottesville, Virginia, April 15-16, 1998. 33–45.